

Steady state solution of warped accretion discs

Lei Chen^{1*}, Shengmiao Wu^{1†} and Feng Yuan^{1‡}

¹ *Key Laboratory for Research in Galaxies and Cosmology, Shanghai Astronomical Observatory, Chinese Academy of Sciences, 80 Nandan Road, Shanghai 200030, China*

19 November 2018

ABSTRACT

We consider a thin accretion disc warped due to the Bardeen-Petterson effect, presenting both analytical and numerical solutions for the situation that the two viscosity coefficients vary with radius as power law, with the two power law indices not necessarily equal. The analytical solutions are compared with numerical ones, showing that our new analytical solution is more accurate than previous one, which overestimates the inclination changing in the outer disc. Our new analytical solution is appropriate for moderately warped discs, while for extremely misaligned disc, only numerical solution is appropriate.

Key words: accretion discs – black hole physics – galaxies: nuclei

1 INTRODUCTION

Observational evidences are accumulating that accretion discs around black holes can be warped. Warped accretion discs have been directly observed by water maser observations in NGC4258 (Miyoshi et al. 1995; Neufeld & Maloney 1995; Herrnstein et al. 1996) and Circinius galaxy (Greenhill et al. 2003). The lack of correlation of radio jets in AGNs and the disc plane of host galaxy (Kinney et al. 2000; Schmitt et al. 2002) can also be explained by disc warping. Wu et al. (2008) discussed the possibility that double-peaked Balmer lines in AGNs be emitted by warped disc. Possible evidence for disc warping is also found in X-ray binaries, including the misalignment between jets and orbital planes in GRO J 1655-40 (Greene et al. 2001; Hjellming & Rupen 1995), and the precessing of jets in SS433 (Blundell & Bowler 2004).

Theoretically, warpping can be caused by various mechanisms, including tidally induced warping by a companion in a binary system (Terquem & Bertout 1993; Larwood et al. 1996; Terquem & Bertout 1996), radiation driven or self-inducing warping, (Maloney et al. 1996; Maloney & Begelman 1997; Maloney et al. 1998; Pringle 1996, 1997), magnetically driven disc warping, (Lai 1999, 2003; Pfeiffer & Lai 2004), and frame dragging driven warping (Bardeen & Petterson 1975). Herein we consider the shape of a disc warped by the last mechanism.

Bardeen & Petterson (1975) pointed out that, the combining effect of Lense-Thirring effect and the viscosity within the disc cause the inner part of the disc to be aligned

with the central black hole, while the outer part of disc remains tilted, thus resulting in a warped disc. Pringle (1992) derived the dynamical equations of such a warped disc. Scheuer & Feiler (1996, hereafter SF96) analytically solved the equation with a first order approximation, assuming constant viscosity coefficients. Lodato & Pringle (2006) numerically solved the equations, also assuming constant viscosity coefficients. Martin et al. (2007, hereafter MPT07) generalized SF96’s analytical solution to the situation that the viscosity coefficients varies as power law, and then, Martin (2008, hereafter M08) used this solution to fit the maser observation of NGC4258’s disc.

We carried on a numerical calculation for a warped disc with power-law varying ν , and compared the results with MPT07’s analytical solution. The importance of this work lies in such a fact: MPT07’s analytical solution (and SF96’s, as well) are based on first order approximation, under the assumption of a small inclination angle $\theta_{out} \ll 1$, while the real accretion discs can be strongly misaligned $\theta_{out} \sim 1$, e.g., the fitting of NGC4258 shows a strong misaligning. A numerical calculation is needed to tell exactly how the error grows. Our calculation shows a prominent deviation between analytical solution and exact solution when the inclination angle are large, suggesting that the analytical solutions not appropriate for study of NGC4258 or other strongly misaligned discs.

We then proposed another way to extrapolate the small θ_{out} solution to large θ_{out} situation, and thus find a new analytical solution. The new solution is also compared with numerical calculation and proves to be more accurate for large θ_{out} situation. We also generalized the analytical solutions to the situation that ν_1 and ν_2 have different power index.

* Email: lchen@shao.ac.cn

† Email: smwu@shao.ac.cn

‡ Email: fyuan@shao.ac.cn

2 THE BASIC SCENARIO AND EQUATIONS

We use the assumptions the same as adopted by Pringle (1992). The disc is assumed to be a thin one, consisting of concentric (but misaligned) circular gas rings. Each ring can be totally described with its surface density Σ , its angular velocity $\boldsymbol{\Omega}$, and its radial velocity V_r . Note that $\boldsymbol{\Omega}$ is a vector, so that it describes both the speed of the rotation $\Omega = |\boldsymbol{\Omega}|$ and the orientation of the ring $\mathbf{l} = \boldsymbol{\Omega}/\Omega$. So, the state of the disc can be totally described by the distribution of the three quantities with radius R , $\Sigma = \Sigma(R)$, $\boldsymbol{\Omega} = \boldsymbol{\Omega}(R)$, and $V_r = V_r(R)$. Each ring will receive viscous torque from neighbouring rings whenever the angular velocity $\boldsymbol{\Omega}$ changes with radius, $\frac{\partial \boldsymbol{\Omega}}{\partial R} \neq 0$. Each ring also receive a Lense-Thirring torque from the central black hole whenever it is misaligned with the black hole. The dynamical equations under such assumption are

$$\begin{aligned}\dot{\Sigma} &= -\frac{1}{R}(R\Sigma V_r)' \\ \dot{\mathbf{L}}_{surf} &= -\frac{1}{R}(RV_r\mathbf{L}_{surf})' + \frac{1}{R}\mathbf{T}_{vis}' + \boldsymbol{\Omega}_{pre} \times \mathbf{L}_{surf} \\ \mathbf{T}_{vis} &= R^3\Sigma(\nu_1\Omega'\mathbf{l} + \frac{\nu_2}{2}\Omega'') \\ \Omega &= \Omega_K\end{aligned}\quad (1)$$

Where $\boldsymbol{\Omega}_{pre}$ is the Lense-Thirring precession frequency

$$\boldsymbol{\Omega}_{pre} = \omega_p/R^3 = \frac{2G\mathbf{J}_H}{c^2R^3}\quad (2)$$

$\mathbf{L}_{surf} = \Sigma\mathbf{L}_s$ is the surface density of angular momentum. $\mathbf{L}_s = R^2\boldsymbol{\Omega}$ is the specific angular momentum, i.e., the angular momentum carried by unit mass. Here we use a dot on the head to stand for $\frac{\partial}{\partial t}$, and the prime symbol “'” to stand for $\frac{\partial}{\partial R}$.

In this work, we use logarithmic coordinate $x = \ln(R/R_0)$, where R_0 is an arbitrarily defined length scale, so that all the physical quantities shall be written as functions of x . The mass of a ring $x \sim x + dx$ is $dm = \Sigma \cdot 2\pi R dx = 2\pi\Sigma_a dx$, where annulus density $\Sigma_a = R^2\Sigma$ is the mass on unit x interval and unit arc angle. The angular momentum of the ring is $d\mathbf{L} = 2\pi\mathbf{L}_a dx = 2\pi\Sigma_a\mathbf{L}_s dx$, where annulus angular momentum density $\mathbf{L}_a = \Sigma_a\mathbf{L}_s$ is the angular momentum on unit x interval and unit arc angle. And we describe the radial motion of rings with $V_x = \frac{1}{R}V_r$, which is the x interval the ring moves in unit time. So the disc can be describe with $(\Sigma_a, \mathbf{L}_a, V_x)$, as functions of x , and the evolution of the disc is described with the evolution of the functions with time t . In the following we use a dot on the head to stand for $\frac{\partial}{\partial t}$, and the prime symbol “'” to stand for $\frac{\partial}{\partial x}$.

With the denotation defined above, the equations can be written in a simpler form (nevertheless equivalent to the previous form).

$$\begin{aligned}\dot{\Sigma}_a &= -(\Sigma_a V_x)' \\ \dot{\mathbf{L}}_a &= (\dot{\mathbf{L}}_a)_{adv} + (\dot{\mathbf{L}}_a)_{vis} + (\dot{\mathbf{L}}_a)_{pre} \\ &= -(V_x\mathbf{L}_a)' + \mathbf{T}_{vis}' + \boldsymbol{\Omega}_{pre} \times \mathbf{L}_a \\ \mathbf{T}_{vis} &= \Sigma_a(\nu_1\Omega'\mathbf{l} + \frac{\nu_2}{2}\Omega'') \\ \Omega &= \Omega_K\end{aligned}\quad (3)$$

Note that the “'” here means $\frac{\partial}{\partial x}$ instead of $\frac{\partial}{\partial R}$, and $\frac{\partial}{\partial x} = R\frac{\partial}{\partial R}$.

3 STEADY STATE SOLUTION FOR SLIGHTLY MISALIGNED DISC

Under Keplerian assumption, the disc can be entirely depicted by a distribution of \mathbf{L}_a . Eliminating redundant variables, eqs.(3) can be rewritten as

$$\begin{aligned}\dot{\mathbf{L}}_a &= -\left(\frac{3}{2}\nu_1\frac{1}{R^2}\mathbf{L}_a\right)' + \left(\frac{\nu_2}{2}\frac{1}{R^2}L_a\mathbf{l}'\right)' \\ &+ \left(3\left(\nu_1\frac{1}{R^2}L_a\right)'\mathbf{l}\right) + \left(\nu_2\frac{1}{R^2}(\mathbf{l}')^2\mathbf{L}_a\right)' \\ &+ \boldsymbol{\Omega}_{pre} \times \mathbf{L}_a\end{aligned}\quad (4)$$

By 1-eq.(4), we get the parallel part of the equation.

$$\begin{aligned}\dot{L}_a &= -\left(\frac{3}{2}\nu_1\frac{1}{R^2}L_a\right)' - \left(\frac{\nu_2}{2}\frac{1}{R^2}L_a\right)(\mathbf{l}')^2 \\ &+ 3\left(\nu_1\frac{1}{R^2}L_a\right)'' + \left(\nu_2\frac{1}{R^2}(\mathbf{l}')^2L_a\right)'\end{aligned}\quad (5)$$

By eq.(4)–1×eq.(5), we get the perpendicular part of the equation.

$$\begin{aligned}L_a\dot{\mathbf{l}} &= -\left(\frac{3}{2}\nu_1\frac{1}{R^2}L_a\right)\mathbf{l}' + \left(\frac{\nu_2}{2}\frac{1}{R^2}L_a\right)'\mathbf{l}' \\ &+ \left(\frac{\nu_2}{2}\frac{1}{R^2}L_a\right)(\mathbf{l}'')_{\perp} + 3\left(\nu_1\frac{1}{R^2}L_a\right)'\mathbf{l}' \\ &+ \left(\nu_2\frac{1}{R^2}(\mathbf{l}')^2L_a\right)\mathbf{l}' + \boldsymbol{\Omega}_{pre} \times \mathbf{L}_a\end{aligned}\quad (6)$$

When the disc is only slightly misaligned, eqs(4) can be linearized. Taking the z-axis along the direction of $\boldsymbol{\Omega}_{pre}$, we have $\mathbf{l} = l_x\mathbf{e}_x + l_y\mathbf{e}_y + l_z\mathbf{e}_z \approx \mathbf{e}_z + \mathbf{l}_{xy}$, where $\mathbf{l}_{xy} = l_x\mathbf{e}_x + l_y\mathbf{e}_y$, when l_x and l_y are small enough for their second-order term to be neglected. Then $\mathbf{l}' = \mathbf{l}'_{xy} = l'_x\mathbf{e}_x + l'_y\mathbf{e}_y$, $\mathbf{l}'' = \mathbf{l}''_{xy} = l''_x\mathbf{e}_x + l''_y\mathbf{e}_y$, and $\mathbf{l}' \cdot \mathbf{l} = (\mathbf{l}')^2 = 0$. Using these approximations, the two parts of the angular momentum equations becomes

$$\begin{aligned}\dot{L}_a &= -\left(\frac{3}{2}\nu_1\frac{1}{R^2}L_a\right)' + \left(3\nu_1\frac{1}{R^2}L_a\right)'' \\ L_a\dot{\mathbf{l}}_{xy} &= -\frac{3}{2}\nu_1\frac{1}{R^2}L_a\mathbf{l}'_{xy} + \left(\frac{\nu_2}{2}\frac{1}{R^2}L_a\mathbf{l}'_{xy}\right)' \\ &+ 3\left(\nu_1\frac{1}{R^2}L_a\right)'\mathbf{l}'_{xy} + \boldsymbol{\Omega}_{pre} \times (L_a\mathbf{l}_{xy})\end{aligned}\quad (7)$$

Further using SF96 and MPT07's symbol $W = l_x + il_y$, where $i = \sqrt{-1}$, the equation become

$$\begin{aligned}\dot{L}_a &= -\left(\frac{3}{2}\nu_1\frac{1}{R^2}L_a\right)' + \left(3\nu_1\frac{1}{R^2}L_a\right)'' \\ L_a\dot{W} &= -\frac{3}{2}\nu_1\frac{1}{R^2}L_aW' + \left(\frac{\nu_2}{2}\frac{1}{R^2}L_aW'\right)' \\ &+ 3\left(\nu_1\frac{1}{R^2}L_a\right)'W' + i\boldsymbol{\Omega}_{pre}L_aW\end{aligned}\quad (8)$$

It is not surprising that the first part is all the same with that for a planary disc. This means for slightly warped disc we can find the solution in two steps. In first step the evolution and distribution of L_a are solved, with the misaligning omitted and the disc looked upon as planary. In second step the inclination at each radius are found, with L_a already known. This two-step method is much easier than finding the exact solution.

To find a steady state solution, we set the left side of eqs.(8) to zero

$$\begin{aligned}0 &= -\left(\frac{3}{2}\nu_1\frac{1}{R^2}L_a\right)' + \left(3\nu_1\frac{1}{R^2}L_a\right)'' \\ 0 &= -\frac{3}{2}\nu_1\frac{1}{R^2}L_aW' + \left(\frac{\nu_2}{2}\frac{1}{R^2}L_aW'\right)' \\ &+ 3\left(\nu_1\frac{1}{R^2}L_a\right)'W' + i\boldsymbol{\Omega}_{pre}L_aW\end{aligned}\quad (9)$$

The solution of L_a are simple

$$\nu_1 L_a = C_0 R^{5/2} + C_1 R^2 \quad (10)$$

where C_0 and C_1 are constants. C_1 is connected with the condition at inner boundary, and always become unimportant when the concerned region are much larger than inner radius. So we discard C_1 and get

$$\nu_1 L_a = C_0 R^{5/2} \quad (11)$$

Substituting the L_a value back, we get

$$0 = \left(\frac{\nu_2}{2\nu_1} R^{1/2} W' \right)' + \frac{i\omega_p}{\nu_1} R^{-1/2} W \quad (12)$$

If ν_1 and ν_2 vary with radius as power law $\nu_1 = \nu_{10}(R/R_0)^{\beta_1} = \nu_{10} \exp(\beta_1 x)$, $\nu_2 = \nu_{20} \exp(\beta_2 x)$, the equation of W becomes

$$\left(\frac{\nu_{20} R_0}{2} \exp[(1/2 + \beta_2 - \beta_1)x] W' \right)' + i\omega_p \exp[(-1/2 - \beta_1)x] W = 0 \quad (13)$$

Physically we have the boundary conditions

$$\begin{aligned} W &\rightarrow 0 & R &\rightarrow 0 \\ W &\rightarrow W_\infty & R &\rightarrow \infty \end{aligned} \quad (14)$$

Solving eq.(13) under such boundary conditions, we get

$$W = f W_\infty \quad (15)$$

where

$$f = \frac{2^{1-n}}{\Gamma(n)} s^n K_n(s)$$

and

$$n = \frac{1/2 + \beta_2 - \beta_1}{1 + \beta_2}$$

and

$$s = \frac{2}{1 + \beta_2} (1 - i) \sqrt{\frac{\omega_p}{\nu_{20} R_0}} \exp\left(-\frac{1 + \beta_2}{2} x\right)$$

and K_n is the n th order modified Bessel function of the second kind. The solution reduces to the MPT07 one (see eq.(24) therein) when the two viscosity coefficients vary with same index $\beta_1 = \beta_2 = \beta$, and further to SF96 solution when $\beta_1 = \beta_2 = 0$.

By defining the warping radius as

$$R_w = \left(\frac{\omega_p}{\nu_{20}} R_0^{\beta_2} \right)^{1/(1+\beta_2)} \quad (16)$$

the parameter s can be written as

$$s = \frac{2}{1 + \beta_2} (1 - i) \left(\frac{R}{R_w} \right)^{-\frac{1+\beta_2}{2}} \quad (17)$$

Hereafter we always set $R_0 = R_w$, i.e., use the warping radius as length unit, thus making the problem scale-free, and turning the equation into

$$s = \frac{2}{1 + \beta_2} (1 - i) \exp\left(-\frac{1 + \beta_2}{2} x\right) \quad (18)$$

It is easy to see that the warping radius thus defined is where the Lense-Thirring precessing timescale and viscosity timescale equals

$$\frac{1}{\Omega_{pre}(R_w)} \equiv \frac{R_w^3}{\omega_p} = \frac{R_w^2}{\nu_2(R_w)} \quad (19)$$

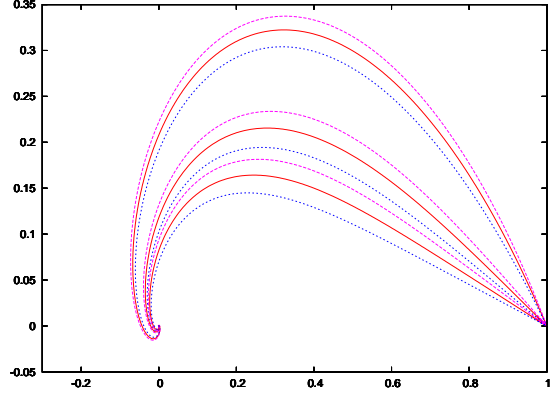


Figure 1. Analytical solutions, l_y/W_∞ against l_x/W_∞ . The solid lines: $\beta_2 = \beta_1$; the long dash lines: $\beta_2 = \beta_1 + 0.1$; the short dash lines: $\beta_2 = \beta_1 - 0.1$. For each line style the three lines are for $\beta_1 = 0, 1, 2$, respectively, from upside to downside.

We present here the analytical solutions for several sets of β_1 and β_2 . The β_1 values are 0, 1, 2, respectively, and for each β_1 we calculated for $\beta_2 = \beta_1$, $\beta_2 = \beta_1 + 0.1$, $\beta_2 = \beta_1 - 0.1$. The plane of z axis and \mathbf{l} at infinite radius, \mathbf{l}_{out} , is set to be the xz plane, so that $\mathbf{l}_{out} = (\sin \theta_{out}, 0, \cos \theta_{out})$ and $W_\infty = \sin \theta_{out}$. For each solution we plot in Fig.1 the f value in the complex plane, which is equivalent to an l_y/W_∞ against l_x/W_∞ plot. In Fig.2 we plot the absolute value and angle of f (divided by 2π) against radius x . The angle of f equals the azimuthal angle φ of \mathbf{l} . The absolute value of f is $|f| = \frac{|W|}{W_\infty} = \frac{\sin \theta}{\sin \theta_{out}}$, and equals $\frac{\theta}{\theta_{out}}$ for small θ_{out} . So Fig.2 is also $\frac{\theta}{\theta_{out}}$ against x and $\frac{\varphi}{2\pi}$ against x plots. We divide φ by 2π so that the value is now the turns \mathbf{l} has precessed around z axis. The very fast growth of φ in the innermost part of disc is not important, because θ is already very small there, meaning the disk is almost aligned with black hole spin.

In the following we call eq.(15) ‘‘solution A’’.

4 NUMERICAL SOLUTION

We developed a finite differential code to solve the evolution of disc. The state of the disc at each time point is represented by the \mathbf{L}_a value upon an uniform grid of x (logarithmic grid of R). The time differential of \mathbf{L}_a are then evaluated, and then the \mathbf{L}_a value at next time point. We used upstream differencing for the advective part in the equation. The code is designed with flexibility to solve various physical problems by adjusting the initial condition and boundary condition.

The code can also be used in finding steady-state solution. If the boundary condition is fixed to the desired setting, and the evolution lasts long enough, in principle the disc will always arrive at the wanted steady state solution. However, the computational cost can be enormous, due to the large time scale range involved in the system. To ensure the solution reached the steady-state value, the time T of disc evolution much be at least several times larger than the viscosity time scale $T > R^2/\nu_1$. On the other hand, the maximum time step Δt to keep the algorithm numerically stable is determined by the time scale for angular momentum viscously diffuse over only one grid, $2\Delta t < \frac{(R*\Delta x)^2}{\nu_1}$, where Δx is the grid size. These two con-

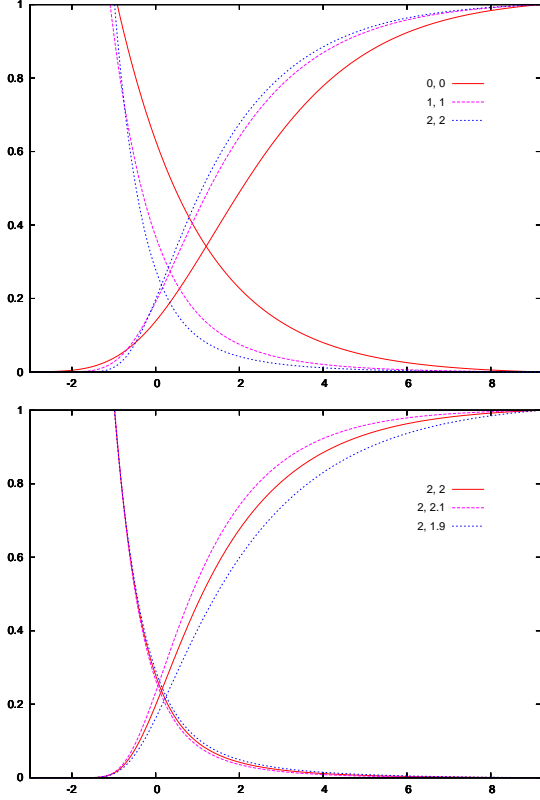


Figure 2. Analytical solutions, $\frac{\theta}{\theta_{out}}$ against x (the ascending lines) and $\frac{\varphi}{2\pi}$ against x (the descending lines). The (β_1, β_2) values are given in the legend. x is defined as $x = \ln(R/R_w)$.

ditions must hold for the whole calculating region R_{in} to R_{out} . So the number of time steps needed are determined by $\left(\frac{R^2}{\nu_1}\right)_{max} / \left(\frac{R*\Delta x^2}{\nu_1}\right)_{min} = \Delta x^{-2} \left(\frac{R_{out}}{R_{in}}\right)^{|2-\beta_1|}$. As an example, supposing $\beta_1 = 0$, $R_{out} = 10^4$, $R_{in} = 10^{-4}$, $\Delta x = 0.01$, we find $T > 10^8 \frac{R_0^2}{\nu_{10}}$, $2\Delta t < 10^{-12} \frac{R_0^2}{\nu_{10}}$, so that the time steps needed are dozens of 10^{20} , absolutely unaffordable. Our way out of this difficulty is artificially add a “speeding up” factor $K(R)$ to the evolutionary equation eq.(4), changing it to

$$\dot{\mathbf{L}}_a = K(R)\mathcal{F}(\mathbf{L}_a) \quad (20)$$

where $\mathcal{F}(\mathbf{L}_a)$ is the time differential of \mathbf{L}_a given in eq.(4). This new equation leads to the right steady-state solution $\mathcal{F}(\mathbf{L}_a) = 0$, though its intermediate results (the \mathbf{L}_a values found before the disc get steady) is physically meaningless. We find $K(R) = R^{2-\beta_1}$ will make the equation converge stably and quickly.

In this work we set a uniform grid of x from $x_{in} = -9.2$ to $x_{out} = 9.2$ (corresponding to $R_{in} \approx 10^{-4}$ and $R_{out} \approx 10^4$, the latter large enough to nearly infinity), and the space resolution $\Delta x = 0.01$. We used a $(\nu_1 \mathbf{L}_a)' = \frac{5}{2} \nu_1 \mathbf{L}_a$ inner boundary condition, by adding a “ghost grid” at $x = x_{in} - \Delta x$, and keep $\mathbf{L}_a(x) = e^{-(2.5-\beta_1)\Delta x} \mathbf{L}_a(x_{in})$, in order to imitate a planary disc obeying $\nu_1 L_a \propto R^{5/2}$ inside of the inner boundary. At the outer boundary we set a fixed $\mathbf{L}_a(x_{out})$, with an inclination angle to black hole spin axis (set as z axis). The plane of z axis and $\mathbf{L}_a(x_{out})$ is set to be xz plane. So $\mathbf{l}(x_{out}) = (\sin \theta_{out}, 0, \cos \theta_{out})$, or $W(x_{out}) = \sin \theta_{out}$. We use

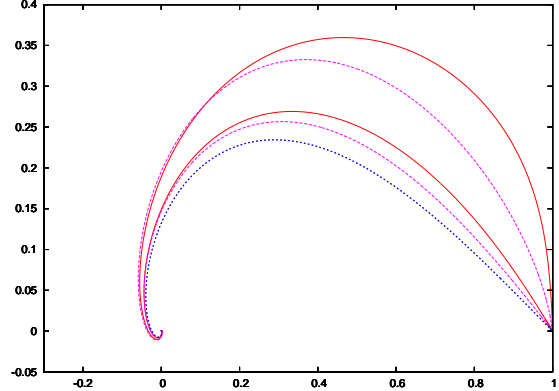


Figure 3. Comparing the analytical and numerical solutions in the l_y/W_∞ against l_x/W_∞ plot. The β values are $\beta_1 = \beta_2 = 3/4$. From upside to downside, the lines are respectively: 1. Numerical solution for $\theta_{out} = 85^\circ$, 2. Solution B for $\theta_{out} = 85^\circ$, 3. Numerical solution for $\theta_{out} = 45^\circ$, 4. Solution B for $\theta_{out} = 45^\circ$, 5. Solution A for all θ_{out} values, and also all the solutions for $\sin \theta_{out} = 0.01$. All lines for solution A coincides, because solution A keeps l_y/W_∞ and l_x/W_∞ constant for different θ_{out} . All lines for $\sin \theta_{out} = 0.01$ almost coincides, showing the error is negligible. In this and following two figures, we use solid lines for numerical solution, long dash lines for solution B, and short dash lines for solution A.

the “solution B” (explained later) as initial condition to save computational cost, though the calculation can converge to steady state solution from arbitrary initial condition.

In Fig.3, Fig.4 and Fig.5, the numerical solution are shown and compared with solution A. As an example, we show the results for $\beta_1 = \beta_2 = 3/4$, and the inclination angle at outer boundary to be $\theta_{out} = \arcsin(0.01)$, 30° , 85° , or equivalently, $W_\infty = 0.01$, 0.5 , 0.9962 . The numerical solution and analytical solution A coincides well when the disc is only slightly misaligned $|W_\infty| \ll 1$, but when the inclination angle is large the two solution deviates strongly. So we conclude that solution A is not appropriate for large inclination angle. In the plot of mass distribution, we use $R^{\beta_1} \Sigma$ because analytical solutions predicts $\Sigma \propto R^{-\beta_1}$ (similar as in planary disc). The numerically calculated mass distribution differs from analytical solution mainly in the vicinity of warping radius, showing a dip there. This is natural because the warping there bring forth additional angular momentum transfer, so that the gas there falls faster than in the planary disc, and thus cause a lower density there.

5 A NEW ANALYTICAL SOLUTION FOR NOT SO SLIGHTLY MISALIGNED DISC

To find a better analytical solution for more strongly misaligned disc, we define another measure of misaligning $V = \theta(\cos \varphi + i \sin \varphi)$, where θ and φ are the inclination angle and azimuthal angle of \mathbf{l} , respectively. To the first order approximation of θ , W and V equals, $W = \sin \theta(\cos \varphi + i \sin \varphi) \approx V$. So all the equations for W in sec.3 also holds for V , hence we write

$$V = fV_\infty = V_\infty \frac{2^{1-n}}{\Gamma(n)} s^n K_n(s) \quad (21)$$

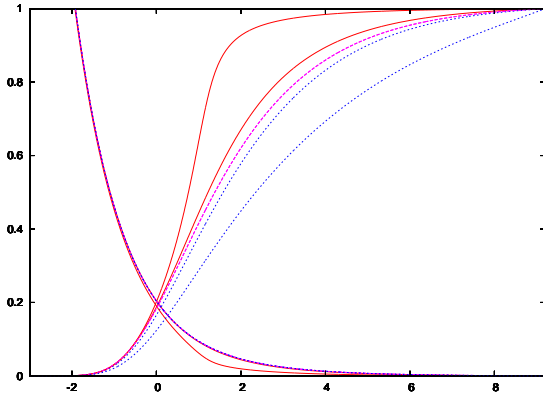


Figure 4. Comparing the analytical and numerical solutions in the $\frac{\theta}{\theta_{out}}$ against x (the ascending lines) and $\frac{\varphi}{2\pi}$ against x (the descending lines) plots. The β values are $\beta_1 = \beta_2 = 3/4$. From upside to downside, the $\frac{\theta}{\theta_{out}}$ lines are respectively: 1. Numerical solution for $\theta_{out} = 85^\circ$, 2. Numerical solution for $\theta_{out} = 45^\circ$, 3. Solution B for all θ_{out} values, and also all the solutions for $\sin\theta_{out} = 0.01$. 4. Solution A for $\theta_{out} = 45^\circ$, 5. Solution A for $\theta_{out} = 85^\circ$. All lines for solution B coincides, because solution A keeps l_y/W_∞ and l_x/W_∞ constant for different θ_{out} . All lines for $\sin\theta_{out} = 0.01$ almost coincides, showing the error is negligible. For $\frac{\varphi}{2\pi}$, the lower line is the numerical solution for $\theta_{out} = 85^\circ$. The upper line is the analytical solutions (solution A and B give same φ , unvarying with θ_{out}), and the numerical solution for $\theta_{out} = 45^\circ$ and $\sin\theta_{out} = 0.01$ also coincide with this.

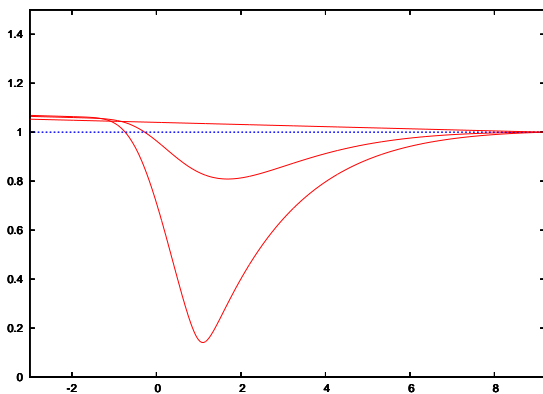


Figure 5. Comparing the analytical and numerical solutions in the $R^{\beta_1}\Sigma$ against x plot. The solid line: numerical solutions, for $\sin\theta_{out} = 0.01$, $\theta_{out} = 45^\circ$, and $\theta_{out} = 85^\circ$, respectively, from upside to downside. The short dash line: analytical solution.

Hereafter we call this “solution B”, and eq.(15) “solution A”. The two solutions is equivalent for slight misalignment, but behave differently when extrapolated to large inclination angle θ_{out} . When θ_{out} varies, solution A keeps $\sin\theta/\sin\theta_{out}$ constant at each R , while solution B keeps θ/θ_{out} constant. Thus solution A causes too quick a decreasing of θ at the outer disc, while solution B gets rid of this backward.

Solution B is plotted in Fig.3 and Fig.4 to compare with solution A and numerical solutions. In the W/W_∞ plot, solution A keeps unchanged with different θ_{out} , while solution B predicts increasing $|W|/W_\infty$ with increasing θ_{out} , which is closer to the numerical results. In the $\theta/\theta_{out} \sim x$ plot, solution B keeps unchanged, while solution A predicts a decreasing θ/θ_{out} with increasing θ_{out} , which contradicts the

numerical results. However, when θ_{out} are so large as 85° , even solution B become very inaccurate. On the other hand, for very small θ_{out} , the two analytical solutions are equivalent and both very accurate.

6 CONCLUSIONS

We generalized MPT07’s analytical solution of warped accretion discs to the situation that the power law index of the two viscosity coefficients is not necessarily equal (solution A). We then proposed a new analytical solution (solution B), which is supposed to be more accurate than solution A. We also presented the numerical solutions of the dynamical equations for warped disc. Our comparison between the two analytical solutions and the numerical results show that solution B is indeed better and is recommendable for moderately or slightly misaligned disc. For extremely misaligned disc, only numerical solution is appropriate. As for the situation in NGC4258, M08’s fitting suggested a large inclination angle, so that numerical solution is needed for more accurate fitting.

ACKNOWLEDGMENTS

This work was supported in part by the Natural Science Foundation of China (grants 10773024, 10833002, 10821302, and 10825314), Bairen Program of Chinese Academy of Sciences, and the National Basic Research Program of China (973 Program 2009CB824800).

REFERENCES

- Bardeen J. M., Petterson J. A., 1975, ApJ, 195, L65
- Blundell K. M., Bowler M. G., 2004, ApJ, 619, L159
- Greene J., Baily C. D., Orosz J. A., 2001, ApJ, 554, 1290
- Greenhill L. J., Kondratko P. T., Lovell J. E. J., Kuiper T. B. H., Moran J. M., Jauncey D. L., Baines G. P., 2003, ApJ, 582, L11
- Herrnstein J. R., Greenhill L. J., Moran J. M., 1996, ApJ, 468, L17
- Hjellming R. M., Rupen M. P., 1995, Nature, 375, 464
- Kinney A. L., Schmitt H. R., Clarke C. J., Pringle J. E., Ulvestad J. S., Antonucci R. R. J., 2000, ApJ, 537, 152
- Lai D., 1999, ApJ, 524, 1030
- Lai D., 2003, ApJ, 591, L119
- Larwood J. D., Nelson R. P., Papaloizou J. C. B., Terquem C., 1996, MNRAS, 282, 597
- Lodato G., Pringle J. E., 2006, MNRAS, 368, 1196
- Maloney P. R., Begelman M. C., 1997, ApJ, 491, L43
- Maloney P. R., Begelman M. C., Nowak M. A., 1998, ApJ, 504, 77
- Maloney P. R., Begelman M. C., Pringle J. E., 1996, ApJ, 472, 582
- Martin R. G., 2008, MNRAS, 387, 830
- Martin R. G., Pringle J. E., Tout C. A., 2007, MNRAS, 381, 1617
- Miyoshi M., Moran J., Herrnstein J., Greenhill L., Nakai N., Diamond P., Inoue M., 1995, Nature, 373, 127
- Neufeld D. A., Maloney P. R., 1995, ApJ, 447, L17
- Pfeiffer H. P., Lai D., 2004, ApJ, 604, 766

- Pringle J. E., 1992, MNRAS, 258, 811
Pringle J. E., 1996, MNRAS, 281, 357
Pringle J. E., 1997, MNRAS, 292, 136
Scheuer P. A. G., Feiler R., 1996, MNRAS, 282, 291
Schmitt H. R., Pringle J. E., Clarke C. J., Kinney A. L.,
2002, ApJ, 575, 150
Terquem C., Bertout C., 1993, A&A, 274, 291
Terquem C., Bertout C., 1996, MNRAS, 279, 415
Wu S.-M., Wang T.-G., Dong X.-B., 2008, MNRAS, 389,
213